

## Supplementary Materials

### CoNi Alloys with Slight Oxidation@N, O Co-doped Carbon: Enhanced Collective Contributions of Cores and Shells to Multifunctional Electrocatalytic Activity and Zn-Air Battery

Xiaobo He <sup>a,b</sup>, Fengxiang Yin <sup>a,b\*</sup>, Guoru Li <sup>a</sup>, Biaohua Chen <sup>a</sup>, Shuo Wang <sup>a</sup>, Mingcheng Gu <sup>a</sup>

<sup>a</sup> Jiangsu Key Laboratory of Advanced Catalytic Materials and Technology, School of Petrochemical Engineering, Changzhou University, Changzhou, 213164, PR China

<sup>b</sup> Changzhou Institute of Advanced Materials, Beijing University of Chemical Technology, Changzhou 213164, PR China

\*Corresponding author

Tel.: +86-519-86330253

E-mail: yinfx@cczu.edu.cn (F. Yin)

## Supplementary Figures and Notes

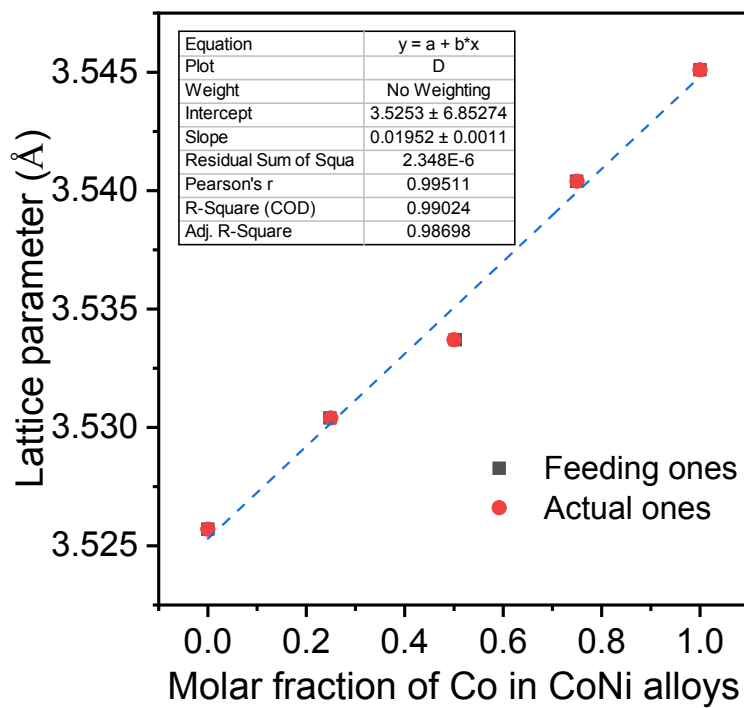


Figure S1. Linear relationship between lattice parameters of the formed CoNi alloys

and molar fractions of Co (the feeding or actual ones).

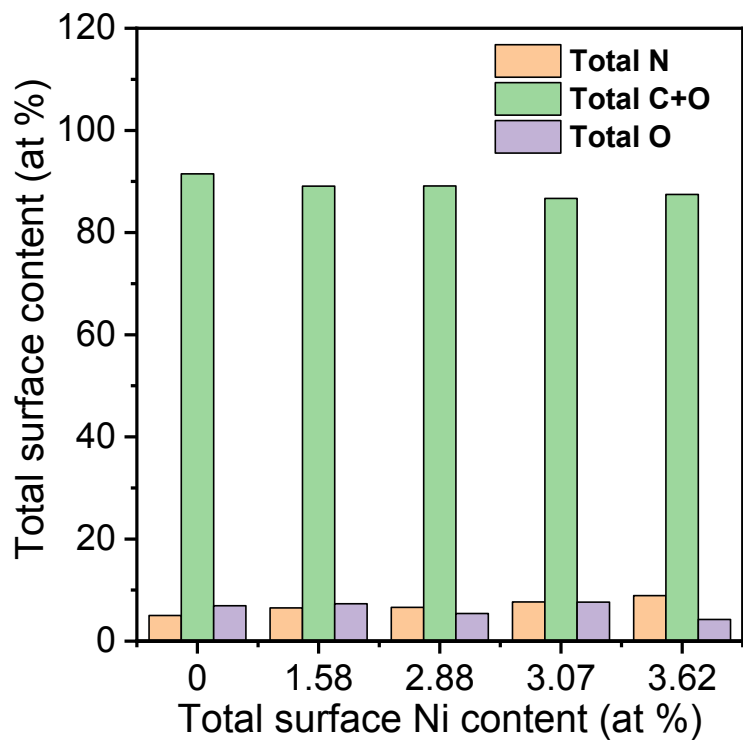


Figure S2. Relationship between total surface Ni content of and others, including total N, total C + O and total O contents.

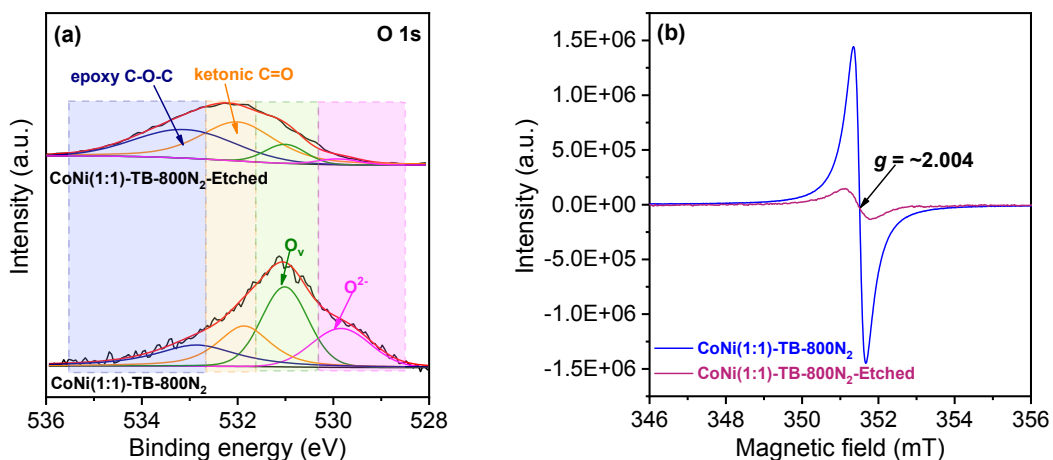


Figure S3. (a) EPR spectra and (b) O 1s XPS spectra of CoNi(1:1)-TB-800N<sub>2</sub> and CoNi(1:1)-TB-800N<sub>2</sub>-Etched. CoNi(1:1)-TB-800N<sub>2</sub>-Etched was obtained from CoNi(1:1)-TB-800N<sub>2</sub> etched for one week by using 1 M H<sub>2</sub>SO<sub>4</sub>, and the H<sub>2</sub>SO<sub>4</sub> solution was renewed every day.

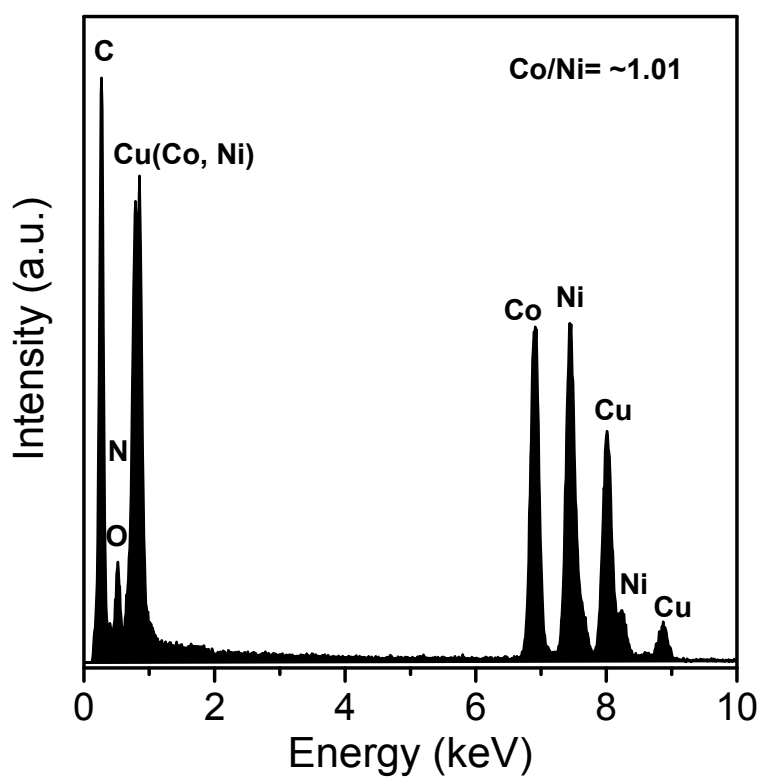


Figure S4. The EDS spectrum of CoNi(1:1)-TB-800N<sub>2</sub>. The signals of Cu came from the used Cu grid for supporting the catalyst during the observation on TEM.

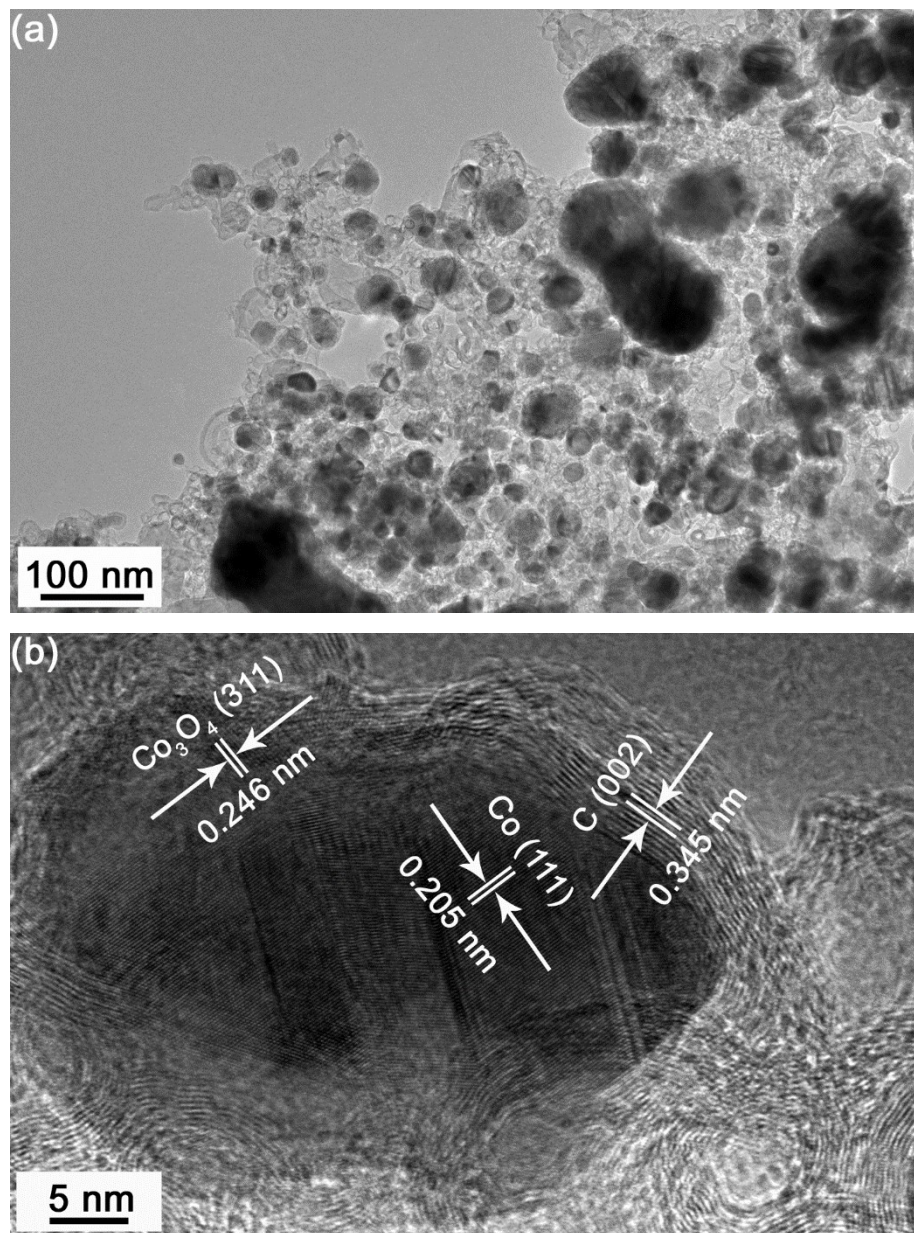


Figure S5. (a) TEM and (b) HRTEM images of Co-TB-800N<sub>2</sub>.

**Note S1:** The presence of  $\text{Co}_3\text{O}_4$  observed in HRTEM is consistent with the results of Raman spectra (Figure 1b) and XPS results of Co 2p (Figure 2a, Table 1 and 2) and O 1s (Figure 2d, Table 1 and 2). Similarly, CoNi(3:1)-TB-800N<sub>2</sub> also contain the small amounts of  $\text{Co}_3\text{O}_4$ , as indicated in Figure S6, Figure 1b, Table 1 and 2.

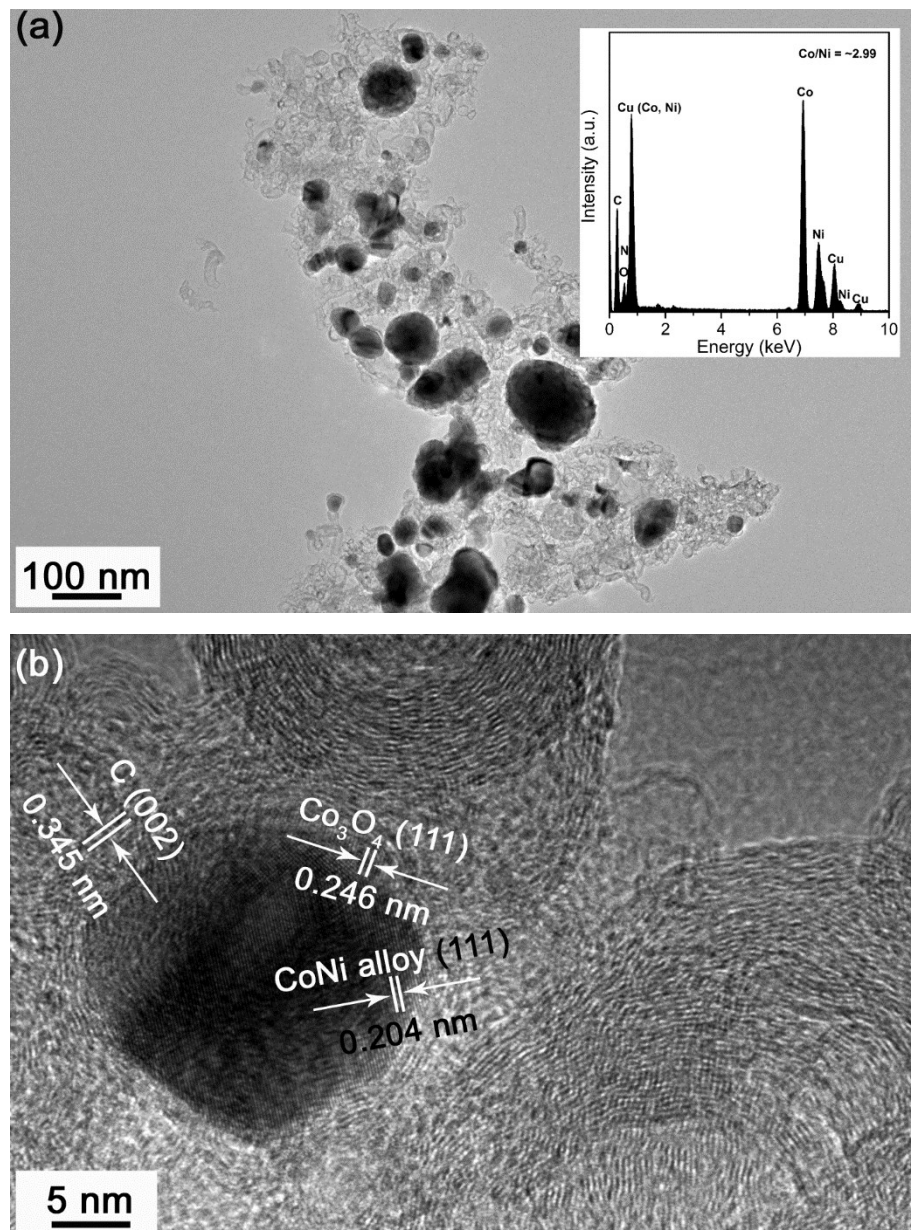


Figure S6. (a) TEM and (b) HRTEM images of CoNi(3:1)-TB-800N<sub>2</sub>. The inset in Figure S3a is the corresponding EDS spectrum.

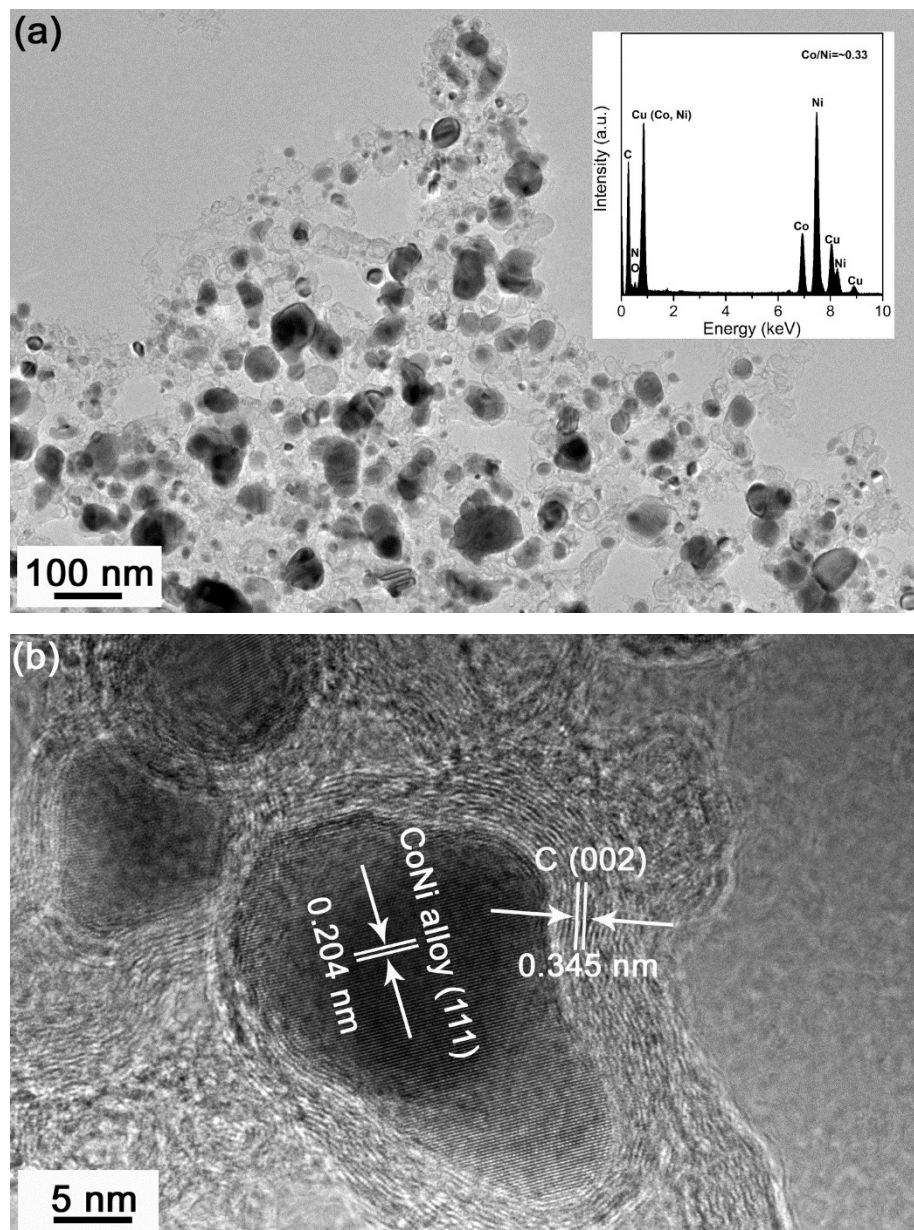


Figure S7. (a) TEM and (b) HRTEM images of CoNi(1:3)-TB-800N<sub>2</sub>. The inset in Figure S4a is the corresponding EDS spectrum.

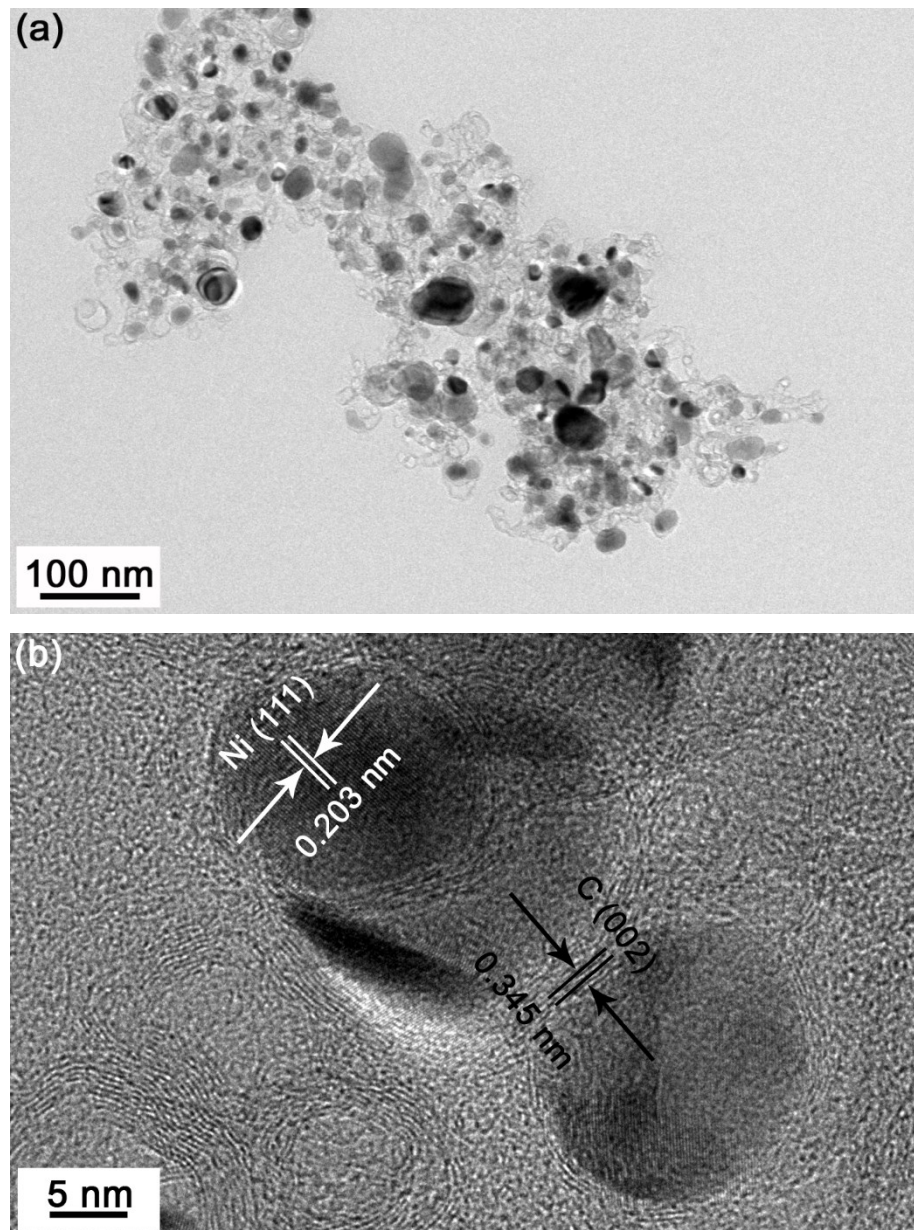


Figure S8. (a) TEM and (b) HRTEM images of Ni-TB-800N<sub>2</sub>.

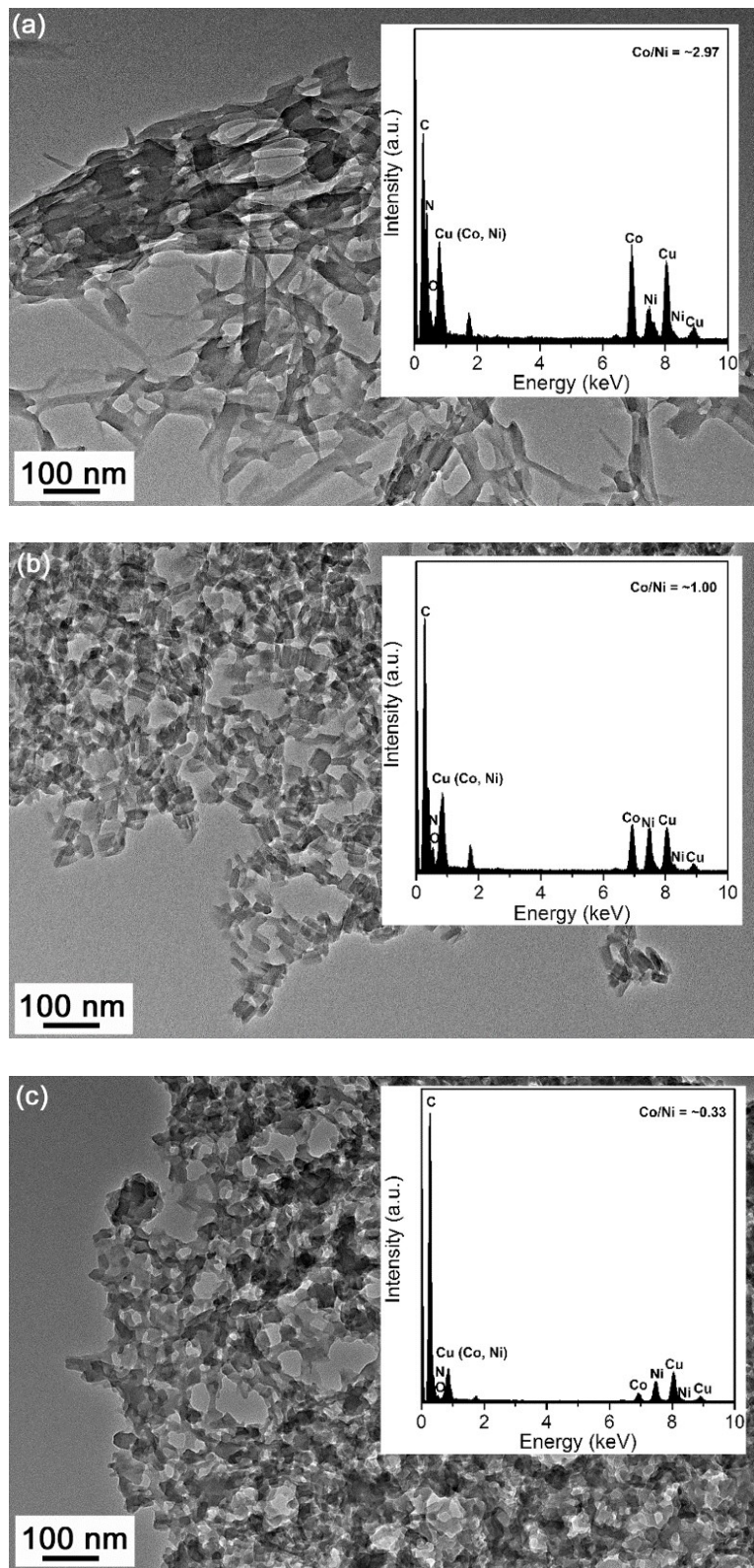


Figure S9. TEM images of the bimetal CoNi-precursors. (a) CoNi(3:1)-precursor. (b) CoNi(1:1)-precursor. (c) CoNi(1:3)-precursor. The insets are their corresponding EDS

spectra.

**Note S2:** These TEM images of the bimetal CoNi-precursors show the net-like nanostructures. Their corresponding EDS results demonstrate that the Co/Ni actual molar ratios are very close to the feeding ones. In addition, the ICP-OES results of these bimetal CoNi-precursors also confirm that the Co/Ni actual molar ratios in them are almost identical with the feeding ones. Specifically, the Co/Ni actual molar ratios of CoNi(3:1)-precursor, CoNi(1:1)-precursor, and CoNi(1:3)-precursor determined by ICP-OES are ~3.02, ~0.98, and ~0.32, respectively. Thus, the results above suggest that the Co/Ni actual molar ratios in the CoNi-precursors are well controlled by the feeding ones, as well as the resulting catalysts with CoNi alloys (Figure S4, S6 and S7).

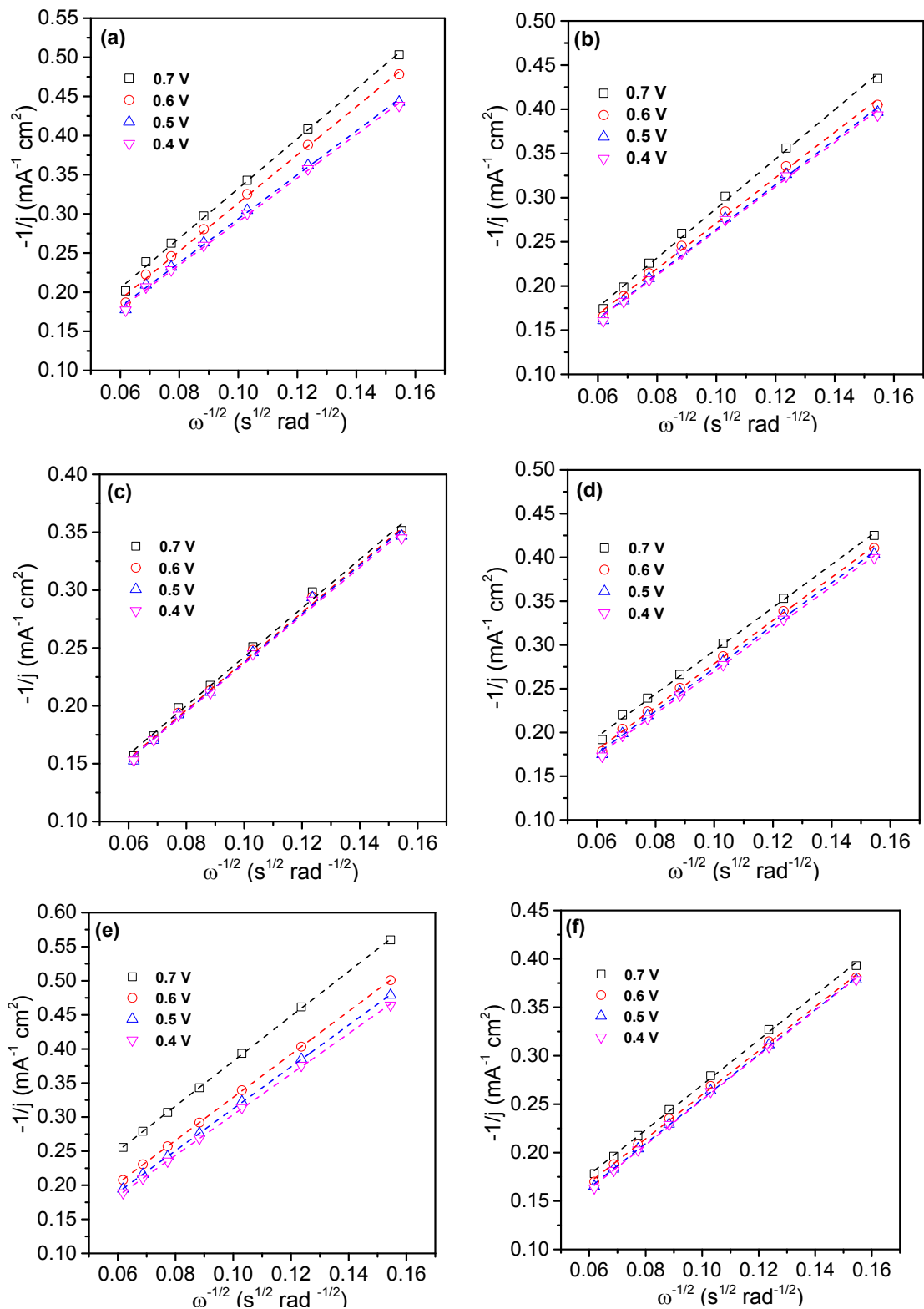


Figure S10. Koutecky-Levich (K-L) plots at various potentials (vs. RHE). (a) Co-TB-800N<sub>2</sub>, (b) CoNi(3:1)-TB-800N<sub>2</sub>, (c) CoNi(1:1)-TB-800N<sub>2</sub>, (d) CoNi(1:3)-TB-800N<sub>2</sub>, (e) Ni-TB-800N<sub>2</sub>, and (f) 20 wt% Pt/C.

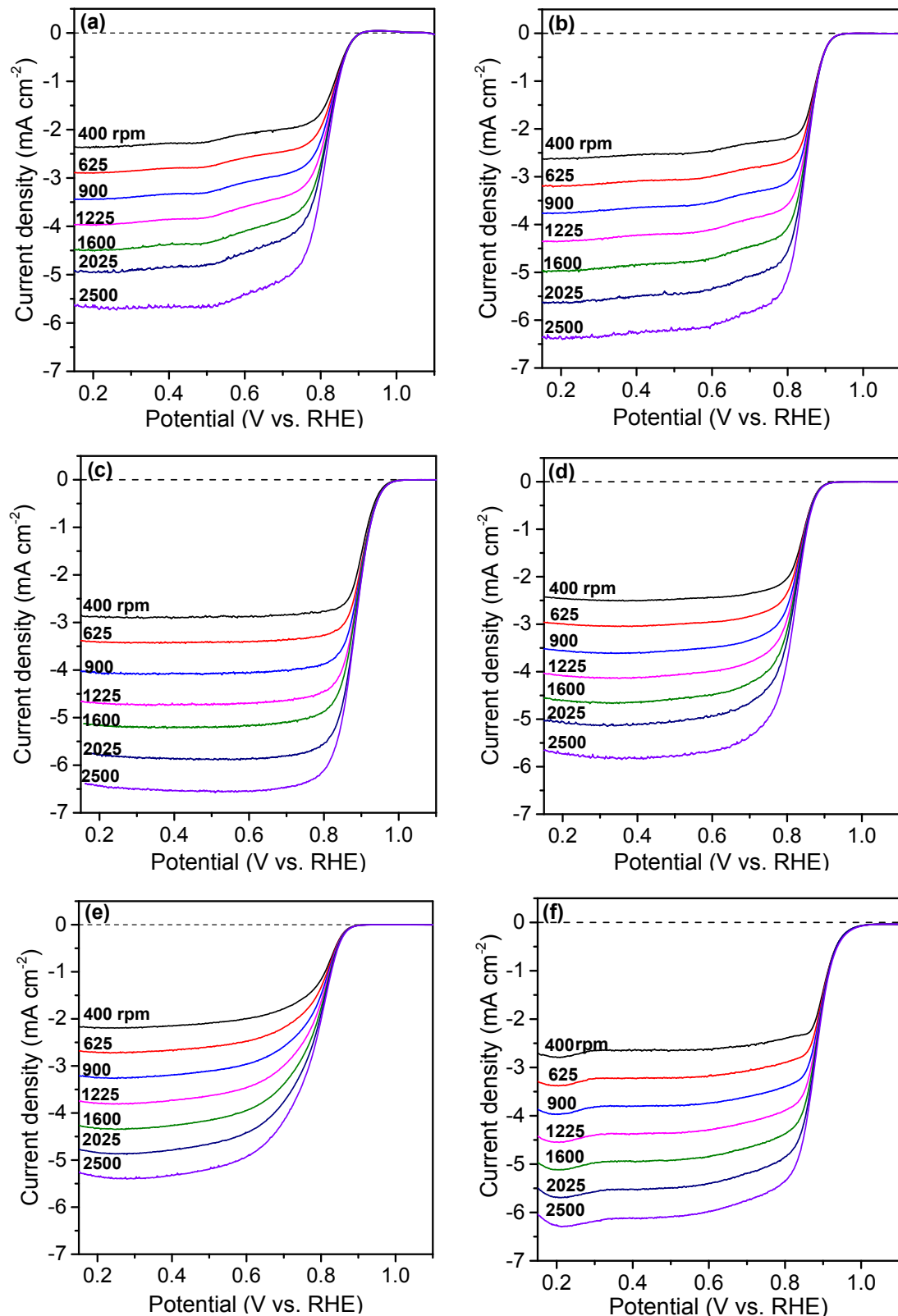


Figure S11. RDE curves at various rotating speeds. (a) Co-TB-800N<sub>2</sub>, (b) CoNi(3:1)-TB-800N<sub>2</sub>, (c) CoNi(1:1)-TB-800N<sub>2</sub>, (d) CoNi(1:3)-TB-800N<sub>2</sub>, (e) Ni-TB-800N<sub>2</sub>, and

(f) 20 wt% Pt/C.

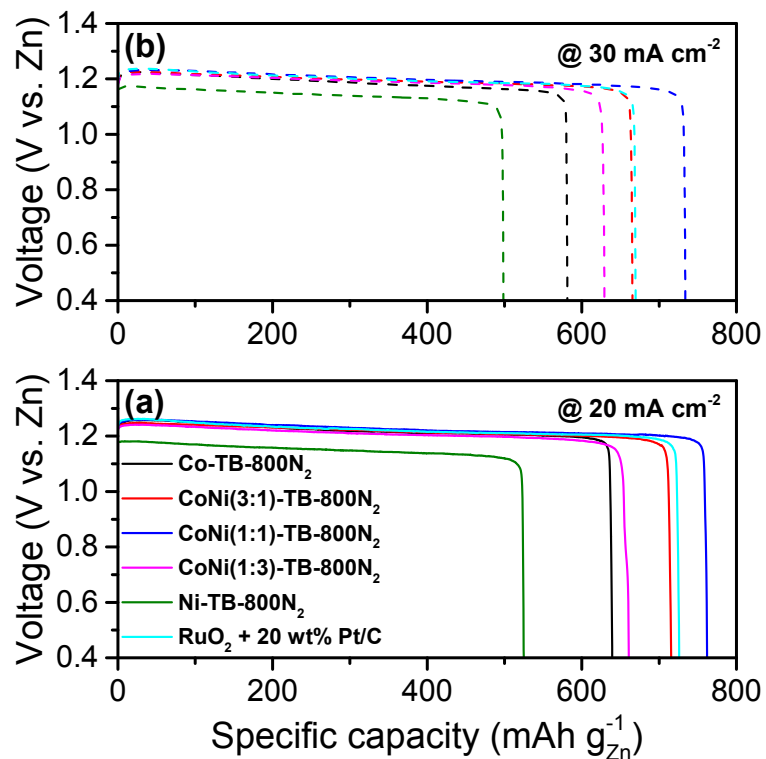


Figure S12. Galvanostatic discharge curves of the primary Zn-air batteries at (a) 20  $\text{mA cm}^{-2}$  and (b) 30  $\text{mA cm}^{-2}$ .

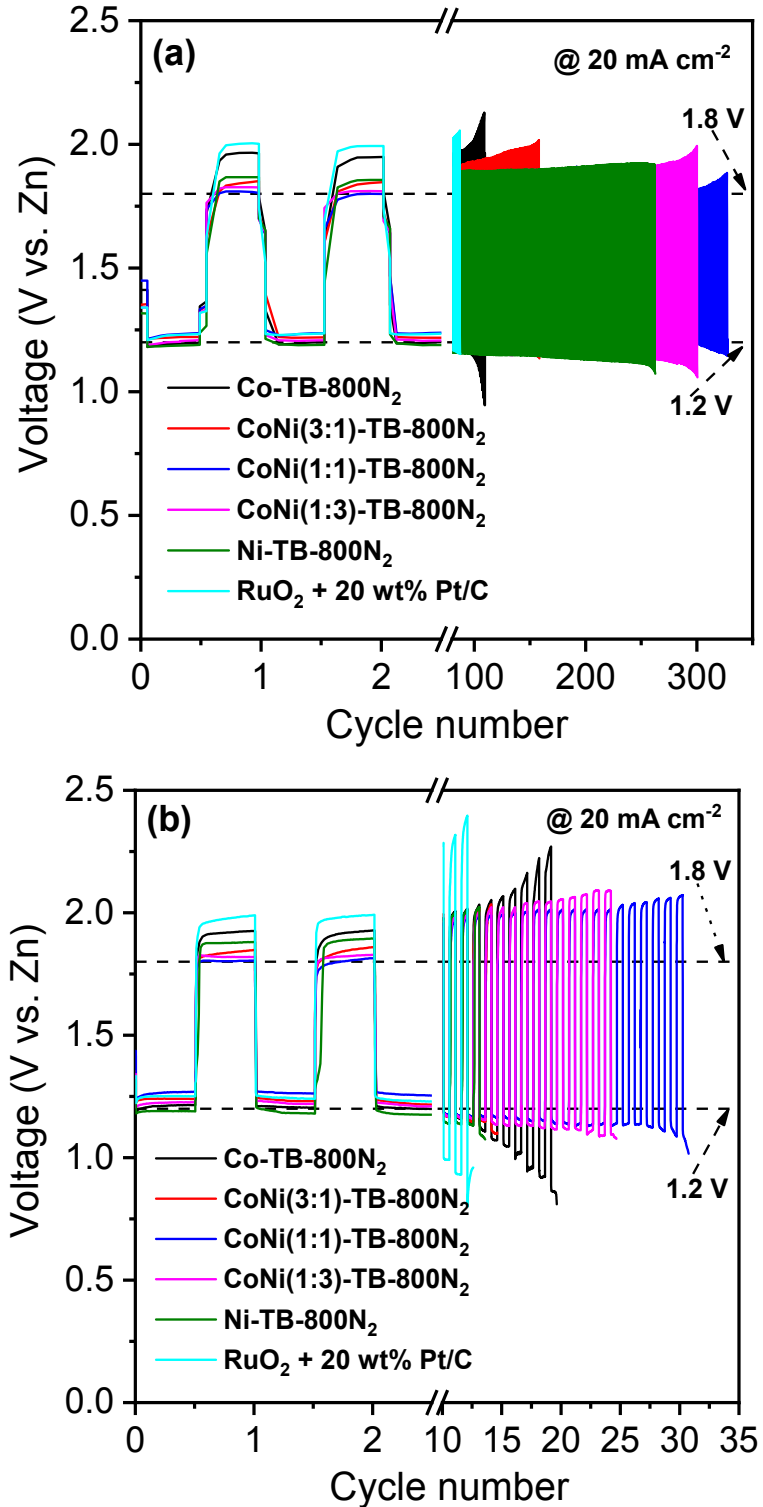


Figure S13. Cycling performance of rechargeable Zn-air batteries at  $20 \text{ mA cm}^{-2}$ . (a) Pulse one with 10 min of discharge and 10 min of charge. (b) Long-time one with 2 h of discharge and 2 h of charge.

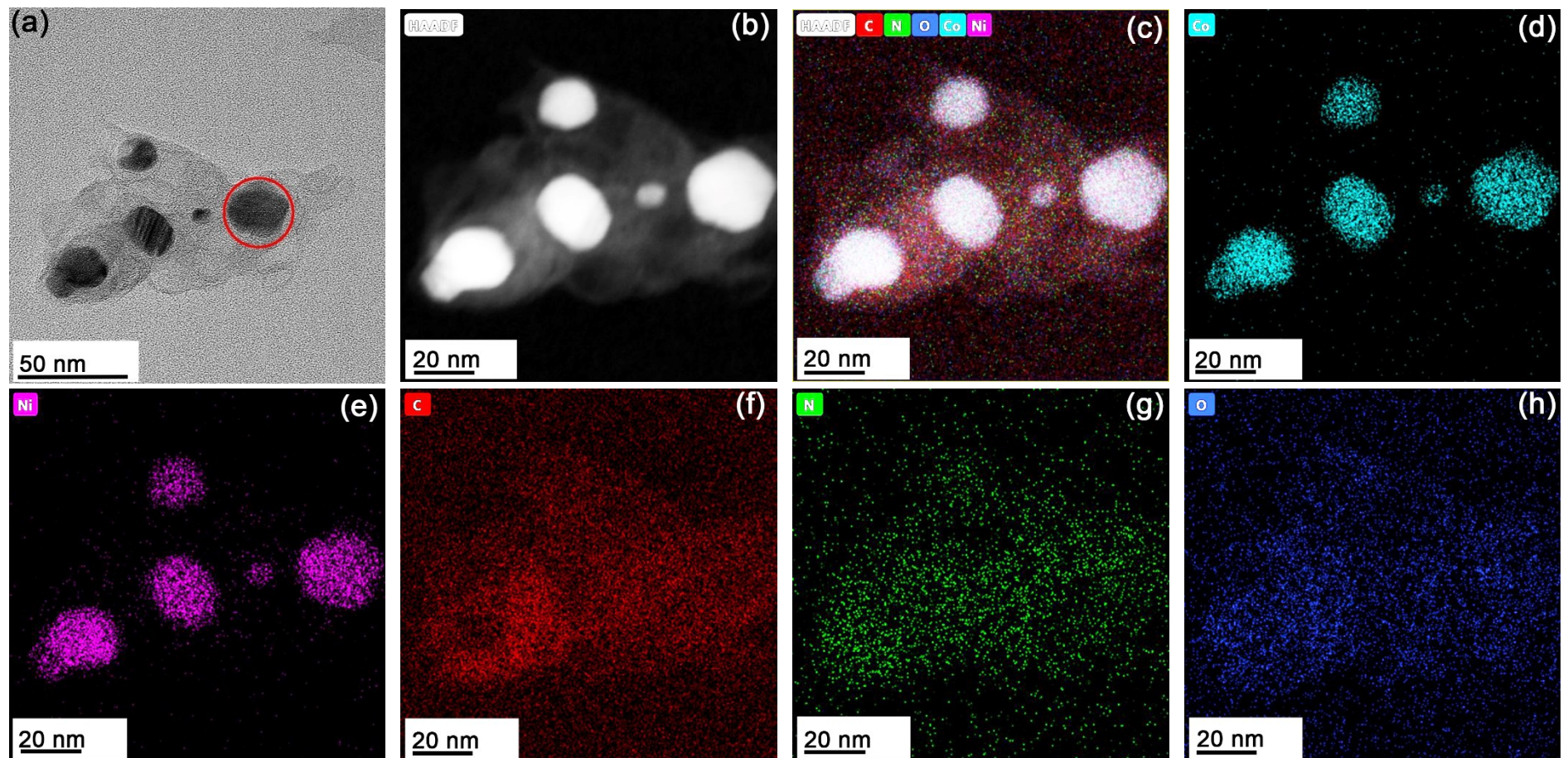


Figure S14. Additional EDS mappings of CoNi(1:1)-TB-800N<sub>2</sub>. (a) TEM image. (b) HAADF image with a higher magnification of 475 kx. (c) Overlapped distribution of Co, Ni, C, N, O and HAADF image. (d)-(h) Distribution of individual elements of Co, Ni, C, N, and O, respectively.

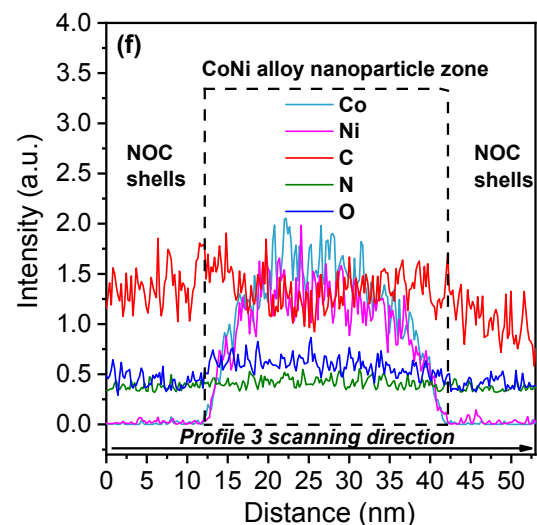
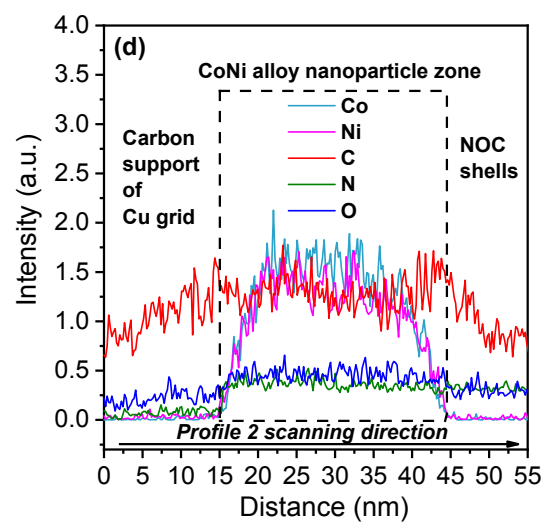
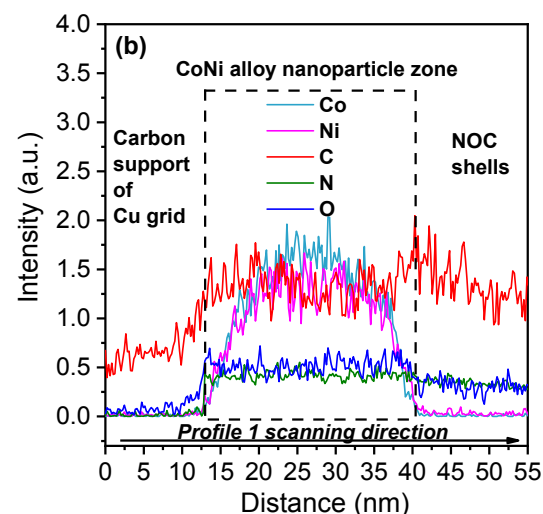
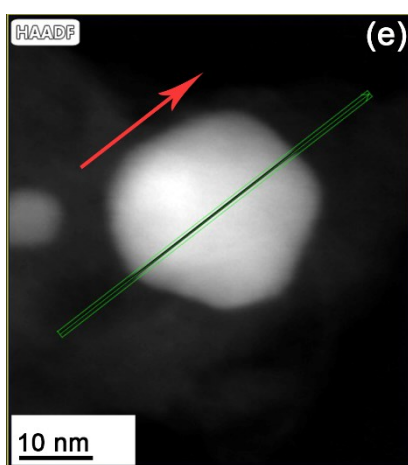
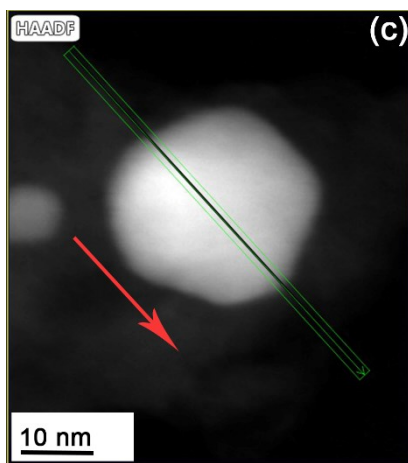
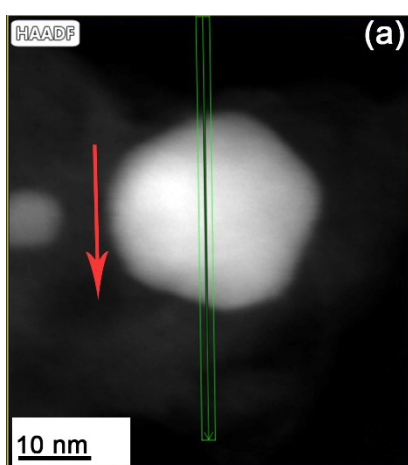


Figure S15. The EDS line scanning across a single CoNi alloy nanoparticle and the surrounding NOC shells from three directions: (a), (c) and (e) HAADF images of the

selected CoNi alloy nanoparticle and the surrounding NOC shells in Figure S14a (marked by a red circle) with a magnification of 950 kx, in which the scanning directions are shown by both red and green arrows. (b), (d) and (f) Corresponding distribution profiles of Co, Ni, C, N and O.

**Note S3:** The additional mappings for the typical CoNi(1:1)-TB-800N<sub>2</sub> were performed (Figure S14), which were collected under the higher magnification (475 kx) as compared those shown in Figure 3 (225 kx). The distributions of Co (Figure S14d) and Ni (Figure S14e) still clearly show that vast majority of them are concentrated in CoNi alloy nanoparticles rather than the outer NOC shells. Furthermore, a single CoNi alloy nanoparticle and the surrounding NOC shells were selected to perform EDS line scanning with a higher magnification of 950 kx than that of additional mappings (485 kx). The results for three scanning directions are shown in Figure S15. Obviously, Co and Ni are mainly distributed in the CoNi alloy nanoparticle, whereas the NOC shells almost do not contain them (Figure S15b, S15d and S15f). Even if there are Co and/or Ni in the NOC shells, their amounts are extreme low.

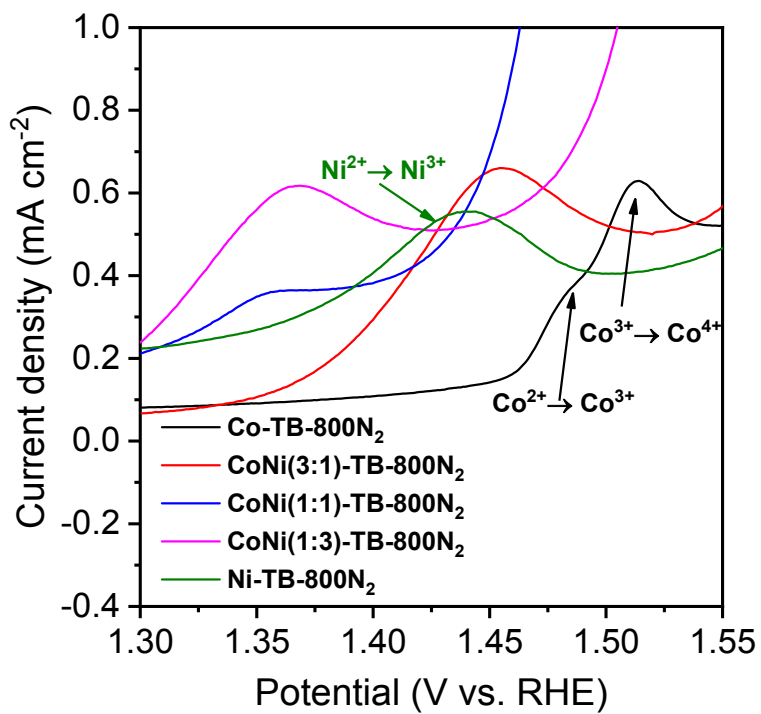


Figure S16. The local OER LSVs for the oxidation waves of the resulting catalysts within the potential range from 1.30 to 1.55 V vs. RHE.

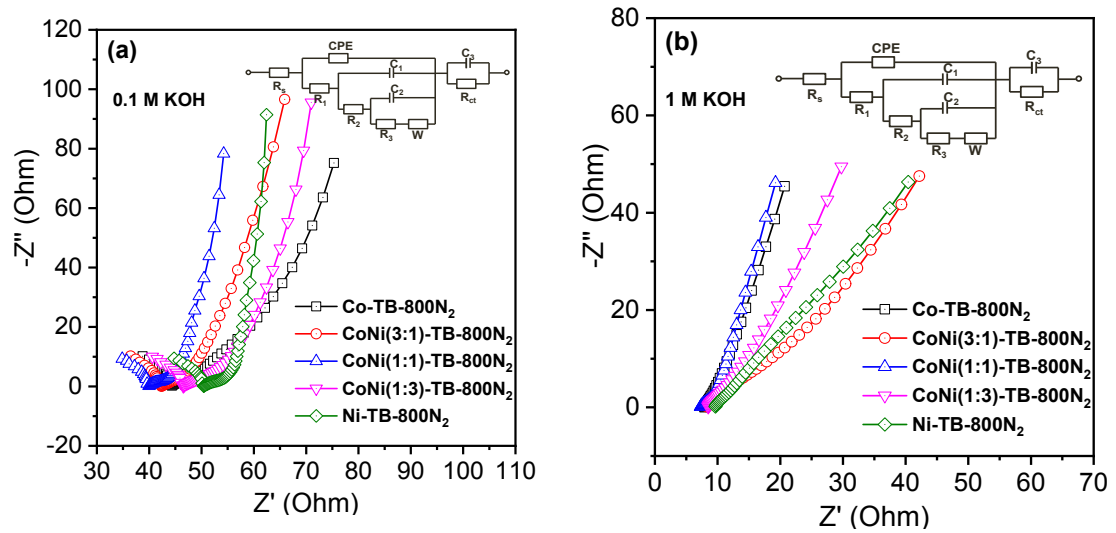


Figure S17. The EIS spectra of the resulting catalysts in (a) 0.1 M KOH and (b) 1 M KOH. The corresponding equivalent circuit is shown in the insets.

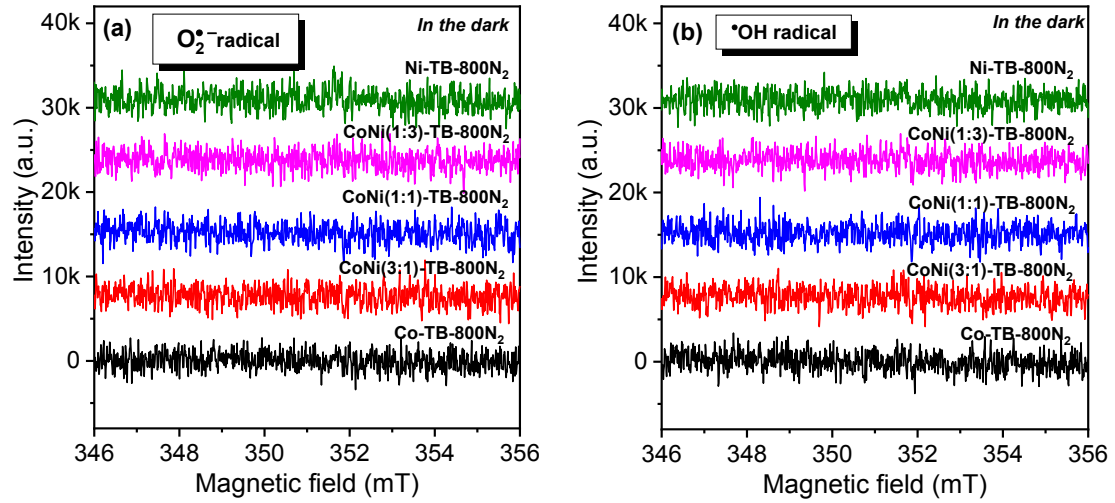


Figure S18. DMPO-EPR spin-trapping spectra of (a)  $\text{O}_2^{\bullet-}$  and (b)  $\cdot\text{OH}$  in the dark.

## Supplementary Tables

Table S1. The BET SSAs, pore sizes and pore volumes of the resulting catalysts.

Catalysts	BET SSA ( $\text{m}^2 \text{ g}^{-1}$ )	Pore size (nm)		Pore volume ( $\text{cm}^3 \text{ g}^{-1}$ )			Total
		Micropore	Mesopore	Micropore	Mesopore	Total	
Co-TB-800N <sub>2</sub>	56.62	1.057	7.63	0.02	0.14	0.16	
CoNi(3:1)-TB-800N <sub>2</sub>	63.07	1.067	15.47	0.02	0.29	0.31	
CoNi(1:1)-TB-800N <sub>2</sub>	70.62	1.086	21.49	0.03	0.39	0.42	
CoNi(1:3)-TB-800N <sub>2</sub>	84.46	1.106	24.36	0.03	0.43	0.46	
Ni-TB-800N <sub>2</sub>	113.52	1.140	27.98	0.05	0.54	0.59	

Table S2. Summary of ORR activity for the recently developed Co and/or Ni/NC typed catalysts <sup>a)</sup>.

Catalyst	Mass loading (mg cm <sup>-2</sup> )	Electrolyte	$E_{1/2}$ (V vs. RHE)	Tafel slope (mV dec <sup>-1</sup> )	References
CoNi(1:1)-TB-800N <sub>2</sub>	0.12	0.1 M KOH	0.888	41	This work
NPCN/CoNi-NCNT	0.71	0.1 M KOH	0.870	54	S1
CoPNi-N/C	0.30	0.1 M KOH	0.840	43	S2
Co@NHCC-800	N.A.	0.1 M KOH	0.837	67	S3
Co/NGC-3	0.20	0.1 M KOH	0.850	61	S4
CoS <sub>x</sub> /Co-NC-800	0.25	0.1 M KOH	0.800	62	S5
Co <sub>2</sub> P/CoN-in-NCNTs	0.10	0.1 M KOH	0.850	49	S6
Co@Co <sub>3</sub> O <sub>4</sub> @NC-900	0.36	0.1 M KOH	0.800	N.A.	S7
NMC/Co@CNTs	0.30	0.1 M KOH	0.791	65	S8

<sup>a)</sup> The ORR activity of the listed catalysts were evaluated on the RDE glassy carbon electrode (GCE).

Table S3. Summary of OER activity for the recently-developed Co and/or Ni/NC typed catalysts <sup>a)</sup>.

Catalyst	Mass loading (mg cm <sup>-2</sup> )	Electrolyte	$\eta_{10}$ (V vs. RHE)	Tafel slope (mV dec <sup>-1</sup> )	References
CoNi(1:1)-TB-800N <sub>2</sub>	0.12	1 M KOH	290	58	This work
NPCN/CoNi-NCNT	0.71	0.1 M KOH	360	165	S1
CoDNi-N/C	0.30	0.1 M KOH	360	72	S2
Co@NHCC-800	N.A.	1 M KOH	282	84	S3
Co/NGC-3	0.20	0.1 M KOH	396	92	S4
CoS <sub>x</sub> /Co-NC-800	0.25	0.1 M KOH	310	96	S5
Co <sub>2</sub> P/CoN-in-NCNTs	0.10	0.1 M KOH	420	N.A.	S6
Co@Co <sub>3</sub> O <sub>4</sub> @NC-900	0.36	1 M KOH	370	94	S7
NMC/Co@CNTs	0.30	0.1 M KOH	500	79	S8
(PrBa <sub>0.5</sub> Sr <sub>0.5</sub> ) <sub>0.95</sub> Co <sub>1.5</sub> Fe <sub>0.5</sub>	0.796	0.1 M KOH	320	74	S9
O <sub>5+δ</sub> /3D porous N-doped					

graphene

NiSAs@ACNTFs 0.30 1 M KOH 250 51 S10

Co-N-C catalyst (DAP- 0.30 1 M KOH 350 60 S11

DAB-

C<sub>4</sub>H<sub>6</sub>O<sub>4</sub>•Co•4H<sub>2</sub>O)

CoO@Co/N-rGO N.A. 0.1 M KOH 420 N.A. S12

---

a) The OER activity of the listed catalysts were evaluated on the RDE glassy carbon electrode (GCE).

Table S4. The summary of primary Zn-air battery performance of the resulting catalysts and the mixture of RuO<sub>2</sub> + 20 wt% Pt/C at high current densities.

Catalysts	Primary battery performance at 20 mA cm <sup>-2</sup>			Primary battery performance at 30 mA cm <sup>-2</sup>		
	Discharge plateau (V vs. Zn)	Specific capacity (mAh g <sup>-1</sup> <sub>Zn</sub> )	Energy density (Wh kg <sup>-1</sup> )	Discharge plateau (V vs. Zn)	Specific capacity (mAh g <sup>-1</sup> <sub>Zn</sub> )	Energy density (Wh kg <sup>-1</sup> )
Co-TB-800N <sub>2</sub>	1.198	639.3	765.9	1.188	581.2	690.5
CoNi(3:1)-TB-800N <sub>2</sub>	1.217	715.5	870.8	1.196	665.6	796.1
CoNi(1:1)-TB-800N <sub>2</sub>	1.223	761.9	931.8	1.200	733.8	880.6
CoNi(1:3)-TB-800N <sub>2</sub>	1.208	660.7	798.1	1.193	629.1	750.5
Ni-TB-800N <sub>2</sub>	1.152	524.9	604.7	1.145	498.6	570.9
RuO <sub>2</sub> +20 wt% Pt/C	1.219	726.1	885.1	1.198	669.6	802.2

Table S5. The summary of rechargeable Zn-air battery performance of the resulting catalysts and the mixture of RuO<sub>2</sub> + 20 wt% Pt/C at 20 mA cm<sup>-2</sup>.

Catalysts	Rechargeable battery performance					
	Pulse cycling			Long-time cycling		
	Initial voltaic efficiency (%)	Final voltaic efficiency (%)	Stable running time (h)/cycle number	Initial voltaic efficiency (%)	Final voltaic efficiency (%)	Stable running time (h)/cycle number
Co-TB-800N <sub>2</sub>	61.6	45.8	36/109	62.3	40.7	76/19
CoNi(3:1)-TB-800N <sub>2</sub>	66.0	56.5	52/158	66.2	53.1	56/14
CoNi(1:1)-TB-800N <sub>2</sub>	68.7	61.0	109/327	69.6	53.9	120/30
CoNi(1:3)-TB-800N <sub>2</sub>	66.7	53.5	100/300	66.8	52.2	96/24
Ni-TB-800N <sub>2</sub>	64.1	56.6	87/262	62.5	55.9	48/12
RuO <sub>2</sub> +20 wt% Pt/C	62.0	56.2	29/87	62.3	38.9	48/12

Table S6. Summary of Zn-air battery performance for the recently-developed Co and/or Ni/NC typed catalysts.

Catalyst	Mass loading (mg cm <sup>-2</sup> )	Electrolyte	Primary Zn-air battery		Rechargeable Zn-air battery		References
			Peak power density (mW cm <sup>-2</sup> )	Specific capacity (mAh g <sup>-1</sup> <sub>Zn</sub> )	Energy density (Wh kg <sup>-1</sup> )	Durability	
CoNi(1:1)-TB-800N <sub>2</sub>	0.65	PAA/KOH (~36 wt%)/H <sub>2</sub> O gel with ~1.60 wt% Zn	154.8	808.5 @ 10 mA cm <sup>-2</sup>	1011.4 @ 10 mA cm <sup>-2</sup>	125 h @ 10 mA cm <sup>-2</sup> (10 min of discharge-charge interval; 136 h @ 10 mA cm <sup>-2</sup> (2 h of discharge-charge interval)	This work

		6 M KOH with			12 h @ 10 mA cm <sup>-2</sup>		
Co@NHCC-800	N.A.	0.2 M zinc acetate	248.0	N.A.	N.A.	(5 min of discharge-charge interval)	S3
		6 M KOH with			120 h @ 5 mA cm <sup>-2</sup>		
Co/NGC-3	0.60	0.2 M zinc acetate	134.4	716 @ 5 mA cm <sup>-2</sup>	847.4 @ 5 mA cm <sup>-2</sup>	(20 min of discharge-charge interval)	S4
		6 M KOH with			90 h @ 5 mA cm <sup>-2</sup>		
CoS <sub>x</sub> /Co-NC-800	1.00	0.2 M ZnCl <sub>2</sub>	103.0	770.4 @ 10 mA cm <sup>-2</sup>	923.5 @ 10 mA cm <sup>-2</sup>	(6 min of discharge-charge interval)	S5
		6 M KOH with			96 h @ 5 mA cm <sup>-2</sup>		
Co <sub>2</sub> P/CoN-in-NCNTs	0.50	0.2 M zinc acetate	194.6	649.6 @ 20 mA cm <sup>-2</sup>	844.5 @ 20 mA cm <sup>-2</sup>	(1 h of discharge-charge interval)	S6

---

					200 h @ 5 mA cm <sup>-2</sup>		
Co@Co <sub>3</sub> O <sub>4</sub> @NC-900	1.50-2.00	6 M KOH	64.0	685.0 @ 5 mA cm <sup>-2</sup>	N.A.	(1 h of discharge- charge interval)	S7
NMC/Co@CNTs	3.00	6 M KOH with 0.2 M zinc acetate	163.0	N.A.	N.A.	40 000 s @ 10 mA cm <sup>-2</sup> (100 s of discharge-charge interval)	S8

---

Table S7. Summary of HER activity for the recently-developed Co and/or Ni/NC typed catalysts <sup>a)</sup>.

Catalyst	Mass loading (mg cm <sup>-2</sup> )	Electrolyte	$\eta_{10}$ (mV)	Tafel slope (mV dec <sup>-1</sup> )	References
CoNi(1:1)-TB-800N <sub>2</sub>	0.12	1 M KOH	114	59	This work
Co <sub>2</sub> P/CoN-in-NCNTs	0.20	0.5 M H <sub>2</sub> SO <sub>4</sub>	98	57	S6
(PrBa <sub>0.5</sub> Sr <sub>0.5</sub> ) <sub>0.95</sub> Co <sub>1.5</sub> Fe <sub>0.5</sub> O <sub>5+δ</sub> /3D porous N-doped graphene	0.796	0.1 M KOH	230	124	S9
NiSAs@ACNTFs	0.30	1 M KOH	49	73	S10
Co-N-C catalyst (DAP-DAB-C <sub>4</sub> H <sub>6</sub> O <sub>4</sub> •Co•4H <sub>2</sub> O)	0.30	1 M KOH	180	59	S11
CoO@Co/N-rGO	N.A.	0.1 M KOH	237	67	S12
Ni <sub>2</sub> P/Co <sub>2</sub> P@NC nanospheres	0.20	1 M KOH	251	82	S13
CoP/NCNT-CP	0.28	1 M KOH	271	96	S14

Co@N-CNTs@rGO	0.50	1 M KOH	108	55	S15
Co@NC/B-NCNTs	0.26	1 M KOH	182	105.4	S16

<sup>a</sup> The OER activity of the listed catalysts were evaluated on the RDE glassy carbon electrode (GCE).

## **Supplementary References**

- S1 Y. Hou, S. Cui, Z. Wen, X. Guo, X. Feng and J. Chen, *Small*, 2015, **11**, 5940-5948.
- S2 Z. Li, H. He, H. Cao, S. Sun, W. Diao, D. Gao, P. Lu, S. Zhang, Z. Guo, M. Li, R. Liu, D. Ren, C. Liu, Y. Zhang, Z. Yang, J. Jiang and G. Zhang, *Appl. Catal., B*, 2019, **240**, 112-121.
- S3 J. Wu, L. Hu, N. Wang, Y. Li, D. Zhao, L. Li, X. Peng, Z. Cui, L.-J. Ma, Y. Tian and X. Wang, *Appl. Catal., B*, 2019, **254**, 55-65.
- S4 J. Li, Y. Kang, D. Liu, Z. Lei and P. Liu, *ACS Appl. Mater. Interfaces*, 2020, **12**, 5717-5729.
- S5 Q. Lu, J. Yu, X. Zou, K. Liao, P. Tan, W. Zhou, M. Ni and Z. Shao, *Adv. Funct. Mater.*, 2019, **29**, 1904481.
- S6 Y. Guo, P. Yuan, J. Zhang, H. Xia, F. Cheng, M. Zhou, J. Li, Y. Qiao, S. Mu and Q. Xu, *Adv. Funct. Mater.*, 2018, **28**, 1805641.
- S7 Z. Guo, F. Wang, Y. Xia, J. Li, A.G. Tamirat, Y. Liu, L. Wang, Y. Wang and Y. Xia, *J. Mater. Chem. A*, 2018, **6**, 1443-1453.
- S8 S. Cai, R. Wang, W. Guo and H. Tang, *Langmuir*, 2018, **34**, 1992-1998.
- S9 Y. Bu, H. Jang, O. Gwon, S. H. Kim, S. H. Joo, G. Nam, S. Kim, Y. Qin, Q. Zhong, S. K. Kwak, J. Cho and G. Kim, *J. Mater. Chem. A*, 2019, **7**, 2048-2054.
- S10 S. Dilpazir, P. Ren, R. Liu, M. Yuan, M. Imran, Z. Liu, Y. Xie, H. Zhao, Y. Yang, X. Wang, C. Streb and G. Zhang, *ACS Appl. Mater. Interfaces*, 2020, **12**, 23017-23027.
- S11 D. Lyu, Y. Du, S. Huang, B. Y. Mollamahale, X. Zhang, S. W. Hasan, F. Yu, S.

- Wang, Z. Q. Tian and P. K. Shen, *ACS Appl. Mater. Interfaces*, 2019, **11**, 39809-39819.
- S12 X. X. Liu, J. B. Zang, L. Chen, L. B. Chen, X. Chen, P. Wu, S. Y. Zhou and Y. H. Wang, *J. Mater. Chem. A*, 2017, **5**, 5865-5872.
- S13 X.-Y. Zhang, B.-Y. Guo, Q.-W. Chen, B. Dong, J.-Q. Zhang, J.-F. Qin, J.-Y. Xie, M. Yang, L. Wang, Y.-M. Chai and C.-G. Liu, *Int. J. Hydrogen Energy*, 2019, **44**, 14908-14917.
- S14 L. Wang, J. Cao, X. Cheng, C. Lei, Q. Dai, B. Yang, Z. Li, M. A. Younis, L. Lei, Y. Hou and K. Ostrikov, *ACS Sustainable Chem. Eng.*, 2019, **7**, 10044-10051.
- S15 Z. Chen, R. Wu, Y. Liu, Y. Ha, Y. Guo, D. Sun, M. Liu and F. Fang, *Adv. Mater.*, 2018, **30**, 1802011.
- S16 Z.-J. Jiang, G. Xie, L. Guo, J. Huang and Z. Jiang, *Electrochim. Acta*, 2020, **342**, 136076.